New Parallel Loaded Resonant Converter With Wide Output Voltage Range

Minjae Kim, Hyeonju Jeong, Byeonggill Han, and Sewan Choi, *Senior Member, IEEE*

***Abstract*—This paper proposes a new parallel loaded resonant converter operating in a narrow switching frequency under wide output voltage range. The proposed converter is capable of operating under zero-voltage switching turn-ON of switches and zero-current switching turn-OFF of diodes. Also, the resonant capacitor with feasible capacitance and current rating can be selected by adjusting the turn ratio of the transformer, making the proposed converter more realizable in high power application. Further, the proposed converter has zero voltage gain at notch resonant frequency, and therefore there are no current and voltage stress in the resonant tank during start-up. Experimental results from a 3-kW prototype are provided to validate the proposed concept.**

***Index Terms*—Parallel loaded resonant converter (PRC), soft switching, wide output voltage range.**

I. Introduction

ECO-FRIENDLY vehicles such as electric vehicles, hybrid electric vehicles, and fuel cell vehicles, and renewable energy sources such as photovoltaic, fuel cells, and wind generation have received significant interest as alternative for fossil fuel depletion, global warming, and environment pollution. Renewable energy sources and electric vehicle batteries generate unregulated output with wide voltage range, and therefore cannot be used in its original form. A dc–dc converter is essential to obtain a regulated and stable output in useful form across the load. Generally, dc–dc converters for this application should be able to achieve high efficiency, high-power density, and high reliability under wide output voltage range [1]–[4].

The dc–dc converter could be either PWM converters such as the phase shift full-bridge converter or resonant converters such as the LLC resonant converter. The phase shift full-bridge converter could achieve zero-voltage switching (ZVS) turn-ON of switches, but the ZVS region can be limited under light load condition. Also, it usually has large turn-OFF switching losses [5]. In contrast, resonant converters have attractive features such as the following: 1) better soft switching characteristic of switches, especially smaller turn-OFF switching loss; 2) utilization of parasitic elements such as leakage and magnetizing inductors of transformer; 3) low electromagnetic interference emissions; and 4) simple structure due to absence of clamp circuits [6]–[15].

The resonant converter can be classified into the series loaded resonant converter (SRC), the parallel loaded resonant converter (PRC), the series-parallel loaded resonant converter (SPRC), and the LLC resonant converter [6]. The SRC could achieve ZVS turn-ON of switches if operated above resonance. However, the main drawbacks of the SRC are that it cannot be controlled at no-load condition and the maximum gain is smaller than 1. Although the PRC has no no-load regulation issue, its circulating energy is much larger than that of the SRC. The SPRC remains the advantages of the SRC and PRC, which are smaller circulating energy and no-load regulation issue.

The LLC resonant converter has been attracting more attention due to the advantages over the aforementioned resonant converters such as small circulating energy and turn-OFF current of switches [8]–[12]. However, under wide output voltage range, the LLC resonant converter may have undesirable problems such as increased transformer size, wide switching frequency variations, and high conduction losses [13]–[15]. Furthermore, the LLC resonant converter has start-up issues: since the voltage gain curve of the LLC resonant converter is relatively flat when the switching frequency is higher than the resonant frequency, high voltage, and current stresses occur at the start-up moment if the start-up switching frequency is not sufficiently high [16]–[20].

Recently, the resonant converters with wide output voltage range have been proposed in the literature [2], [4], [13], [21]–[30]. The design and control methods based on the LLC resonant converter were introduced in [2], [4], and [21]. However, the operating switching frequency range is still wide under wide voltage range. Some topologies and/or hybrid switching method (pulse frequency modulation plus phase shift) have been proposed for narrow switching frequency range at the expense of increased component counts, thereby reducing power density and efficiency of system [22]–[30]. Also, the hybrid method increases control complexity and implementation difficulty by handling two control variables [31].

In this paper, a new resonant converter with notch resonant tank is proposed for wide output voltage range application. The proposed converter has the following features: 1) narrow operating switching frequency range under very wide output voltage

Manuscript received December 30, 2016; revised March 15, 2017; accepted May 4, 2017. Date of publication May 19, 2017; date of current version January 3, 2018. This work was supported by the Human Resources Development of the Korea Institute of Energy Technology Evaluation and Planning (KETEP) grant funded by the Korea government Ministry of Trade, Industry, and Energy (20154030200720). Recommended for publication by Associate Editor Y. Xing. *(Corresponding Author: Sewan Choi.)*

M. Kim is with the Department of New Energy Engineering, Seoul National University of Science and Technology, Seoul 139-743, Korea (e-mail: tostood@seoultech.ac.kr).

H. Jeong, B. Han and S. Choi are with the Department of Electrical & Information Engineering, Seoul National University of Science and Technology, Seoul 139-743, Korea (e-mail: hyeonju0618@seoultech.ac.kr; byeonggill@seoultech.ac.kr; schoi@seoultech.ac.kr).

Color versions of one or more of the figures in this paper are available online at http://ieeexplore.ieee.org.

Digital Object Identifier 10.1109/TPEL.2017.2706360

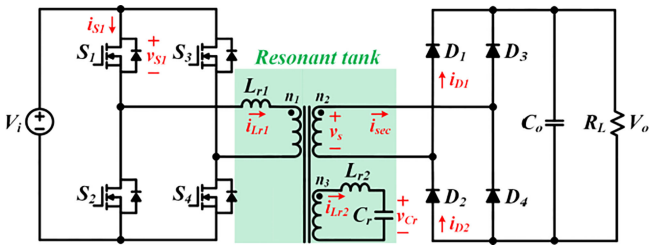

Fig. 1. Generalized circuit diagram of the proposed converter.

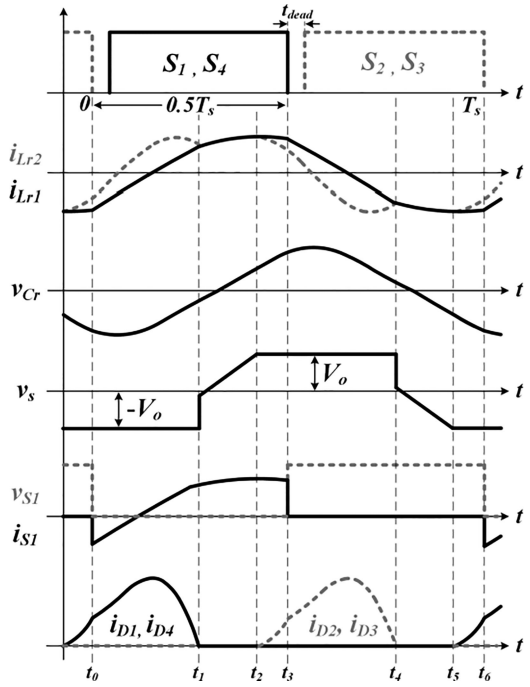

Fig. 2. Key waveforms of the proposed converter.

range; 2) ZVS turn-ON of switches and zero-current switching (ZCS) turn-OFF of diodes regardless of voltage and load variation; 3) easy selection of the resonant capacitor by utilizing a tertiary winding of the transformer; and 4) no voltage and current stress in the resonant tank during start-up. A 3-kW prototype of the proposed converter has been built and tested to verify the validity of the proposed converter.

II. Proposed Converter

Fig. 1 shows the generalized circuit diagram of the proposed converter. The resonant tank of the proposed converter is composed resonant inductor L_{r1} at the primary side that is connected in series to the transformer and notch resonant tank $L_{r2} - C_r$ that is connected in parallel to the transformer. The output voltage of the proposed converter is regulated by fixed duty cycle and variable switching frequency.

A. Operating Principles

Figs. 2 and 3 show key waveforms and operation states of the proposed converter, respectively. The operation states of the proposed converter are described as follows.

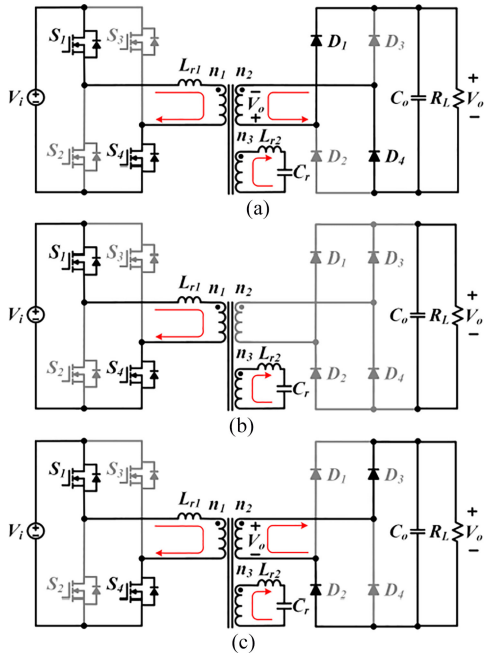

Fig. 3. Operation states of the proposed converter. (a) Mode 1 ($t_0 \sim t_1$). (b) Mode 2 ($t_1 \sim t_2$). (c) Mode 3 ($t_2 \sim t_3$).

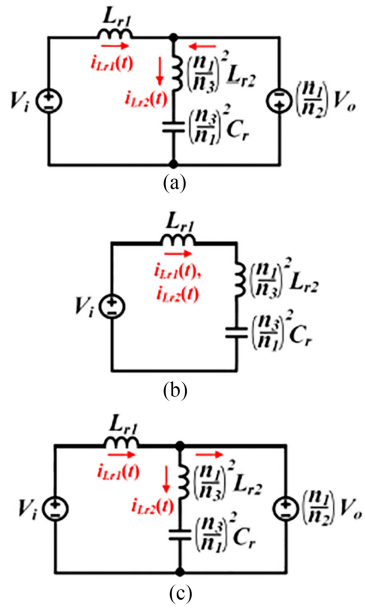

Fig. 4. Equivalent resonant circuits. (a) Mode 1 ($t_0 \sim t_1$). (b) Mode 2 ($t_1 \sim t_2$). (c) Mode 3 ($t_2 \sim t_3$).

Mode 1 ($t_0 - t_1$): This mode begins when switches S_2 and S_3 are turned OFF, making the body diodes of S_1 and S_4 turn ON. In this mode the tertiary side starts resonating with the equivalent circuit shown in Fig. 4(a), transferring power to the load. Current i_{Lr1} is determined by the following equation:

$$i_{Lr1}(t) = \frac{V_i + (n_1 V_o / n_2)}{L_{r1}}(t - t_0) + i_{Lr1}(t_0), t_0 < t < t_1. \quad (1)$$

The current and voltage of resonant components are determined, respectively, as follows:

$$i_{Lr2}(t) = \left(-\frac{n_3}{n_2}V_o - v_{Cr}(t_0)\right)\sqrt{\frac{C_r}{L_{r2}}}\sin\left(\omega_{r1}(t-t_0)\right) + i_{Lr2}(t_0)\cos\left(\omega_{r1}(t-t_0)\right), \quad t_0 < t < t_1 \tag{2}$$

$$v_{Cr}(t) = -\frac{n_3}{n_2}V_o + \left(\frac{n_3}{n_2}V_o + v_{Cr}(t_0)\right)\cos\left(\omega_{r1}(t-t_0)\right) + i_{Lr2}(t_0)\sqrt{\frac{L_{r2}}{C_r}}\sin\left(\omega_{r1}(t-t_0)\right), \quad t_0 < t < t_1 \tag{3}$$

where $\omega_{r1} = 1/\sqrt{L_{r2}C_r}$.

This mode ends when current i_{Lr1} becomes equal to i_{Lr2}. Note that switches S_1 and S_4 are turned ON with ZVS and diodes D_1 and D_4 are turned OFF with ZCS.

Mode 2 ($t_1 - t_2$): In this mode the primary side starts resonating with the equivalent circuit shown in Fig. 4(b). The current and voltage of resonant components are determined, respectively, as follows:

$$i_{Lr1}(t) = i_{Lr2}(t) = \frac{(V_i - v_{Cr}(t_1))}{Z_r}\sin\left(\omega_{r2}(t-t_1)\right) + i_{Lr1}(t_1)\cos\left(\omega_{r2}(t-t_1)\right), \quad t_1 < t < t_2 \tag{4}$$

$$v_{Cr}(t) = \frac{n_3}{n_1}V_i - \left(\frac{n_3}{n_1}V_i - v_{Cr}(t_1)\right)\cos\left(\omega_{r2}(t-t_1)\right) + \frac{n_3}{n_1}i_{Lr1}(t_1)Z_r\sin\left(\omega_{r2}(t-t_1)\right), \quad t_1 < t < t_2 \tag{5}$$

where $\omega_{r2} = 1/\sqrt{((n_3/n_1)^2 L_{r1} + L_{r2})C_r}$ and $Z_r = \sqrt{(L_{r1} + (n_1/n_3)^2 L_{r2})/(n_3/n_1)^2 C_r}$.

During this mode the power is not transferring to the load and the output filter capacitor supplies the load. This mode ends when V_s becomes equal to V_o.

Mode 3 ($t_2 - t_3$): During this mode, again, the tertiary side starts resonating with the equivalent circuit shown in Fig. 4(c), transferring power to the load. Current i_{Lr1} is determined by the following equation:

$$i_{Lr1}(t) = \frac{V_i - (n_1V_o/n_2)}{L_{r1}}(t-t_2) + i_{Lr1}(t_2), \quad t_2 < t < t_3. \tag{6}$$

The current and voltage of resonant components are determined, respectively, as follows:

$$i_{Lr2}(t) = \left(\frac{n_3}{n_2}V_o - v_{Cr}(t_2)\right)\sqrt{\frac{C_r}{L_{r2}}}\sin\left(\omega_{r1}(t-t_2)\right) + i_{Lr2}(t_2)\cos\left(\omega_{r1}(t-t_2)\right), \quad t_2 < t < t_3 \tag{7}$$

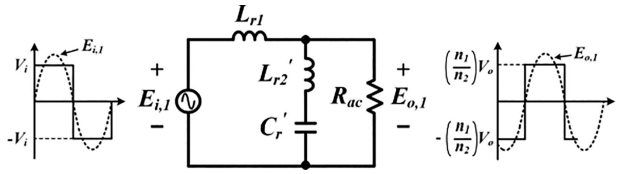

Fig. 5. AC equivalent circuit referred to the primary side.

$$v_{Cr}(t) = \frac{n_3}{n_2}V_o - \left(\frac{n_3}{n_2}V_o - v_{Cr}(t_2)\right)\cos\left(\omega_{r1}(t-t_2)\right) + i_{Lr2}(t_2)\sqrt{\frac{L_{r2}}{C_r}}\sin\left(\omega_{r1}(t-t_2)\right), \quad t_2 < t < t_3. \tag{8}$$

This mode ends when switches S_1 and S_4 are turned OFF. The other half of a cycle is repeated in the same fashion.

B. Voltage Gain Expression

Based on the first-harmonic approximation, the ac equivalent circuit referred to the primary side is shown in Fig. 5. The ac equivalent resistance $R_{\rm ac}$, the fundamental components of the input and output voltage of the resonant tank, and their ratio can be expressed, respectively, as follows:

$$R_{\rm ac} = \left(\frac{n_1}{n_2}\right)^2\frac{8}{\pi}R_L \tag{9}$$

$$E_{i,1}(t) = \frac{4}{\pi}V_i\sin(\omega_s t) \tag{10}$$

$$E_{o,1}(t) = \frac{n_1}{n_2}\frac{4}{\pi}V_o\sin(\omega_s t - \phi) \tag{11}$$

$$\frac{E_{o,1}(t)}{E_{i,1}(t)} = \frac{n_1}{n_2}\frac{V_o}{V_i} = \frac{(j\omega_s L'_{r2} + 1/j\omega_s C'_r)\,||R_{\rm ac}}{j\omega_s L_{r1} + (j\omega_s L'_{r2} + 1/j\omega_s C'_r)\,||R_{\rm ac}} \tag{12}$$

where $L'_{r2} = (n_1/n_3)^2 L_{r2}$ and $C'_r = (n_3/n_1)^2 C_r$.

From (12), the voltage gain of the proposed converter is determined by

$$G = \frac{V_o}{V_i} = \frac{n_2}{n_1}\frac{1}{\sqrt{\left(k\frac{{f_n}^2}{{f_n}^2-1} + 1\right)^2 + \left(\frac{k f_n}{Q}\right)^2}} \tag{13}$$

$$Q = R_{\rm ac}\sqrt{C'_r/L'_{r2}} \tag{14}$$

$$f_{r1} = 1/2\pi\sqrt{L'_{r2}C'_r} \tag{15}$$

$$f_n = f_s/f_{r1} \tag{16}$$

$$k = L_{r1}/L'_{r2}. \tag{17}$$

The voltage gain curves versus normalized frequency for different values of Q, with $k = 2$ is shown in Fig. 6(a). A higher Q leads to a higher slope of the gain curve. It should be noted that a load-independent operation with zero gain occurs at the notch resonance frequency f_{r1}, and therefore output voltage regulation in Region 2 under wide voltage and load variation is desirable, as shown in Fig. 6(a). Fig. 6(b) shows the curves of

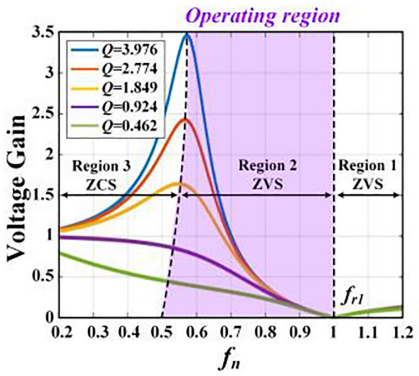

(a)

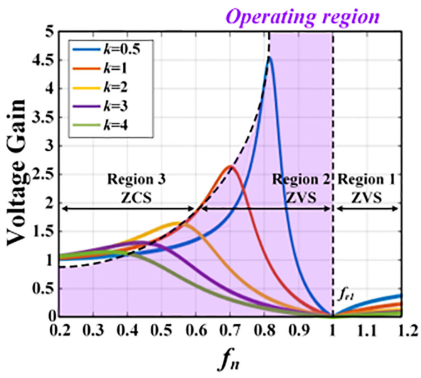

(b)

Fig. 6. Voltage gain curve of the proposed converter. (a) At different Q values with $k = 2$. (b) At different k values with $Q = 1.849$.

TABLE I
DESIGN SPECIFICATIONS

Parameter	Value
Input voltage range	380 V
Output voltage range	50 ∼ 430 V
Maximum output power	3 kW
Maximum output current	7 A
Switching frequency range	80 ∼ 200 kHz

the voltage gain plotted over normalized frequency for different values of k, with $Q = 1.849$. It is seen that operating frequency range becomes narrow as k decreases.

C. Design Procedure

In this section, a design procedure of the proposed converter is presented with an example. A specification for the design example is given in Table I. As shown in Fig. 7, the charging profile can be divided into trickle current (TC) mode, constant-current (CC) mode, and constant-voltage (CV) mode. The TC mode with a constant charging current I_L of 10% rated value is performed if the battery is in a deeply depleted status owing to either over-discharging or extended storage time. When the battery voltage reaches voltage V_L, the charger goes into the CC mode. During the CC mode, the charger charges the battery with maximum charging current I_H while monitoring the

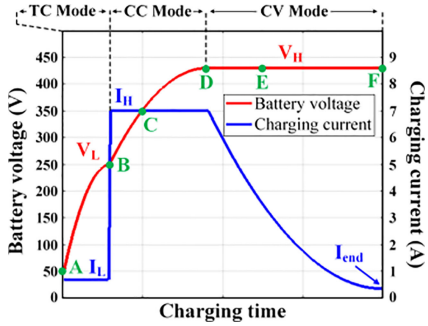

Fig. 7. Example of charging profile.

TABLE II
BATTERY EQUIVALENT RESISTANCES OF OPERATING POINTS ACCORDING TO THE CHARGING PROFILE

	A	B	C	D	E	F
$V_{\rm bat}$	50 V	250 V	350 V	430 V	430 V	430 V
$I_{\rm bat}$	0.7 A	7 A	7 A	7 A	3.5 A	0.35 A
$R_{\rm eq}$	71.4 Ω	35.7 Ω	50 Ω	61.4 Ω	112.8 Ω	1228 Ω
Q	3.289	1.644	2.302	2.829	5.658	56.58
f_{sw}	152.9	91.5	89.4	88.1	97.6	100

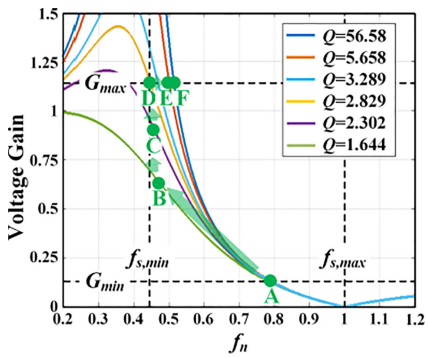

Fig. 8. Trajectory according to the charging profile in the voltage gain curve of the proposed converter.

battery voltage. When the battery voltage reaches up to voltage V_H, the charger goes into the CV mode and then decreases the charging current to current $I_{\rm end}$. Due to the battery's different operating modes, it is necessary to design a battery charger that can respond to the battery charge profile. The design procedure is given in the following three steps.

1) Select Resonant Frequency f_{r1}: In order to ensure ZVS turn-ON of switches and operate with narrow switching frequency range under wide voltage range, the proposed converter should be operated under Region 2, as shown in Fig. 6(a). Therefore, maximum switching frequency $f_{s,\max}$ is chosen to be f_{r1}.

2) Determine Values of Resonant Components: The battery equivalent resistances of operating points on the charging profile shown in Fig. 7 are listed in Table II. Fig. 8 shows a trajectory according to the charging profile in the voltage gain curve of the proposed converter. It is shown that the proposed converter is able to achieve zero voltage gain regardless of Q value due to notch resonant tank, and maximum gain according to Q value

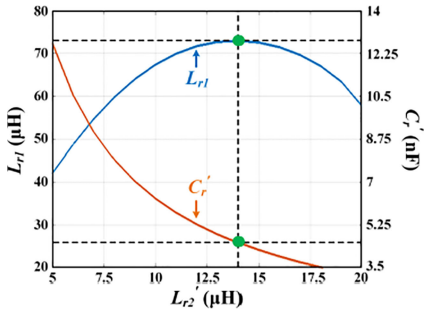

Fig. 9. Resonant inductances and capacitance that meet the design specifications at point D.

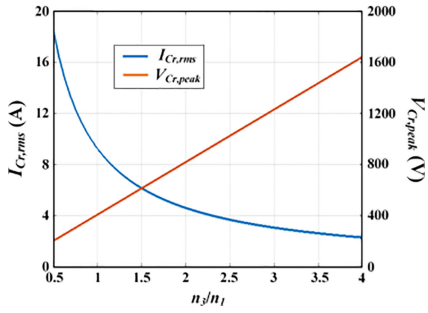

Fig. 10. Voltage and current ratings of resonant capacitor C_r with different values of n_3/n_1.

decreases as Q decreases. Assuming that the battery is in the most deeply depleted status, the required voltage gain is minimum, and the charger starts to operate at point A. During the TC mode, the battery voltage is increased and the switching frequency is decreased. When the battery voltage reaches point B, the charger goes into the CC mode. In the CC mode the switching frequency of the charger is slightly decreased as the battery voltage is increased. When the switching frequency reaches point D, the charger goes into the CV mode. It is noted that the switching frequency at point D is minimum. In the CV mode, the charging current is gradually decreased and the switching frequency is increased. When the battery is fully charged at point F, the charger stops charging. In order to meet the design specifications, the switching frequency at point D is chosen to be minimum switching frequency $f_{s,\min}$ of the charger. Considering a 20% gain margin to avoid Region 3, the required gain at point D is maximum. Note that the turn ratio n_2/n_1 is chosen to be unity since the proposed resonant tank is capable of operating under wide voltage range. The ac equivalent resistance at point D can be expressed as

$$R_{\mathrm{ac},D} = \frac{8}{\pi} R_{\mathrm{eq},D}. \tag{18}$$

By applying f_{r1} and (18) to (14), the quality factor at point D can be expressed as

$$Q_D = \frac{4R_{\mathrm{eq},D}}{\pi^2 f_{s,\max} L'_{r2}}. \tag{19}$$

From (13), (19), $f_{s,\min}$ and $f_{s,\max}$, the required voltage gain at point D can be obtained by

$$G_{\mathrm{req}} = G(L_{r1}, L'_{r2}) = \frac{1}{\sqrt{\left(\frac{L_{r1}}{L_{r2}'}\frac{{f_{s,\min}}^2}{{f_{s,\min}}^2 - {f_{s,\max}}^2} + 1\right)^2 + \left(\frac{2\pi f_{s,\min} L_{r1}}{R_{\mathrm{ac,worst}}}\right)^2}}. \tag{20}$$

Fig. 9 shows the values of resonant inductances and capacitance that meet the design specifications at point D. Since the current rating and turn-OFF current of switches reduce as L_{r1} increases as shown in (1), L_{r1} is chosen to be maximum value to minimize the losses, and resonant values L_{r1}, L'_{r2}, and C'_r are determined by 73 μH, 14 μH, and 50.4 nF, respectively, as shown in Fig. 9. The magnetizing inductance L_m is 1.02 mH.

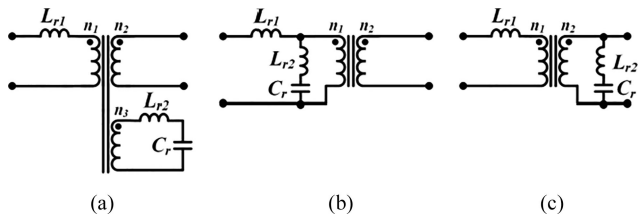

Fig. 11. Connection method of the notch resonant tank in case of (a) $n_1 \neq n_3$ and $n_2 \neq n_3$ (b) $n_1 = n_3$ (c) $n_2 = n_3$.

TABLE III
DESIGN OF RESONANT CAPACITOR WITH AND WITHOUT TERTIARY WINDING

Parameter	With Tertiary Winding [Fig. 2(a)]	Without Tertiary Winding [Fig. 2(b) or (c)]
Turn ratio of transformer	1:1:2	1:1
Peak voltage of C_r	1350 V	675 V
RMS current of C_r	5.85 A	11.7 A
Capacitance of C_r	12.6 nF	50.4 nF
Realization of C_r (from ICEL)	Series connection of five 0.1 μF and two 0.068 μF	Series connection of ten 0.47 μF
Total volume of C_r	26 391 mm^3	95 567 mm^3

The leakage inductances L_{k1-3} are 1.91, 1.19, and 6.56 μH, respectively. The leakage inductance is used as a part of the resonant inductor.

3) Select Tertiary Winding Turn Ratio: The voltage and current rating of resonant capacitor C_r of the proposed converter can be adjusted by the tertiary winding turn ratio of the transformer. From Fig. 5, input impedance and fundamental current of L_{r1} can be expressed, respectively, as

$$Z_i = j\omega_s L_{r1} + (j\omega_s L'_{r2} + 1/j\omega_s C'_r) \,||R_{\mathrm{ac}} \tag{21}$$

$$i_{Lr1,1}(t) = E_{i,1}(t)/Z_i. \tag{22}$$

From (22), the fundamental current and voltage of resonant capacitor at the tertiary side can be expressed as, respectively,

$$i_{Cr,1}(t) = \frac{n_1}{n_3}\frac{R_{\mathrm{ac}}}{R_{\mathrm{ac}} + j\omega_s L'_{r2} + 1/j\omega_s C'_r} i_{Lr1,1}(t) \tag{23}$$

$$v_{Cr,1}(t) = \frac{1}{C_r}\int i_{Cr,1}(t)dt. \tag{24}$$

TABLE IV
PERFORMANCE COMPARISON BETWEEN THE CONVENTIONAL RESONANT CONVERTERS AND THE PROPOSED CONVERTER UNDER WIDE OUTPUT VOLTAGE RANGE

Specifications : Power = 3kW, V_{in} = 380V, V_o = 50 ~ 430V					
	SRC	PRC	LCC	LLC	Proposed
Voltage gain curve	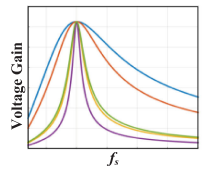	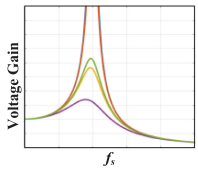	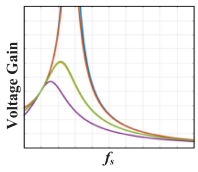	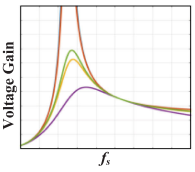	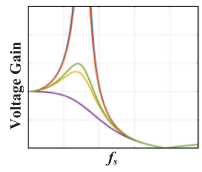
Equivalent resonant circuit	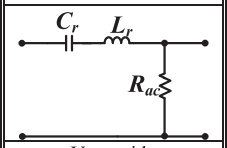	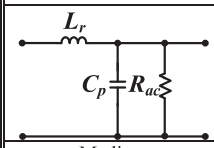	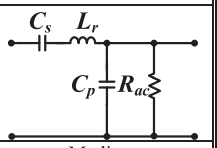	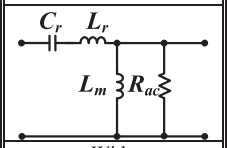	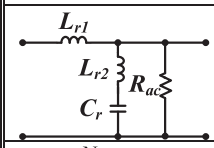
Operating freq. range	Very wide (84kHz ~370kHz)	Medium (85kHz ~181kHz)	Medium (85kHz ~187kHz)	Wide (118kHz ~334kHz)	Narrow (85kHz ~155kHz)
Switching char.	MOSFETs : ZVS turn-on	MOSFETs : ZVS turn-on	MOSFETs : ZVS turn-on	MOSFETs : ZVS turn-on	MOSFETs : ZVS turn-on
	Diodes : ZCS turn-off	Diodes : Hard switching off	Diodes : Hard switching off	Diodes : ZCS turn-off	Diodes : ZCS turn-off
No-load voltage control	Difficulty	Easy	Easy	Easy	Easy
Circulating current	Very small	Large	Medium	Small	Medium
Soft start-up	Difficult	Difficult	Difficult	Difficult	Easy

From (23) and (24), RMS current and peak voltage of resonant capacitor C_r can be approximated, respectively, as in the following:

$$I_{Cr,\mathrm{rms}} \approx I_{Cr,1,\mathrm{rms}} \tag{25}$$

$$V_{Cr,\mathrm{peak}} \approx V_{Cr,1,\mathrm{peak}}. \tag{26}$$

In the application such as EV chargers where the power density is a critical requirement, the switching frequency of the converter is preferred to be high, which leads to high resonance frequency when the resonant converter is employed. This forces the resonant capacitance to be a low value while having high current capability. However, a capacitor with low capacitance, in general, has low current capability. Therefore, a lot of capacitors may need to be connected in series and/or parallel to satisfy low capacitance and high current requirement of the resonant capacitor, resulting in increased volume.

Fig. 10 shows voltage and current rating of resonant capacitor C_r according to turn ratio n_3/n_1. As we can see, as the turn ratio increases, the current rating of the resonant capacitor decreases while increasing its voltage rating. Fig. 11 shows three connection methods of the notch resonant tank according to the turn ratio. Use of the tertiary winding is not mandatory, and the notch resonant tank can be connected directly to the primary winding or the secondary winding if the tertiary winding is not chosen to be used. However, the number of capacitors could significantly be reduced by utilizing the tertiary winding. Table III shows design of the resonant capacitor with and without the tertiary winding. Note that volume of the resonant capacitor has been reduced by 72% by utilizing the tertiary winding.

TABLE V
COMPONENT RATINGS AND SELECTED DEVICES

Components		Rating	Selected Devices
Switches $S_1 \sim S_4$	V_{pk}	380 V	IXTH62N65X2
	I_{rms}	8.1 A	
Diodes $D_1 \sim D_4$	V_{pk}	430 V	DSEI60-06A
	I_{avg}	3.5 A	
Resonant inductor L_{r1}	Inductance	73 μH	Ferrite core PQ50/50
	I_{rms}	11.4 A	
Resonant inductor L_{r2}	Inductance	56 μH	Ferrite core PQ40/40
	I_{rms}	5.7 A	
Resonant capacitor C_r	Capacitance	12.6 nF	
	V_{pk}	1363 V	
	I_{rms}	5.7 A	
Transformer T_r	Turn ratio	13:13:26	Ferrite core EIC90/55
Magnetizing inductor L_m	Inductance	1.02 mH	–
Leakage inductor L_{k1}	Inductance	1.91 μH	–
L_{k2}		1.19 μH	
L_{k3}		6.56 μH	
Output capacitor C_o	Capacitance	9 uF	C4BTHBX4900ZALJ
	V_{pk}	430 V	

D. Performance Comparison Between the Conventional Resonant Conveters and the Proposed Converter

In order to compare the proposed converter to the conventional resonant converters, the conventional resonant converters has been designed under wide output voltage range (50–430 V), and the comparison results are summarized in Table IV.

The SRC has small circulating current at light load in contrast with others. However, the switching frequency should be increased a lot to regulate output voltage at light load, resulting in very wide operating frequency range. Therefore, An SRC is

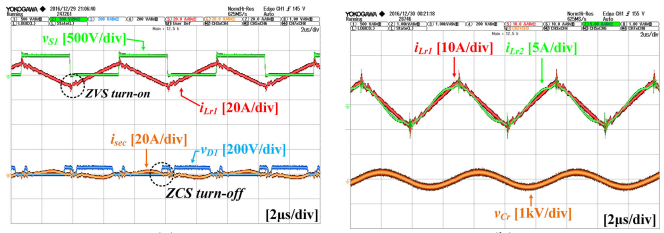

(a) (b)

Fig. 12. Experimental waveforms at $V_o = 50$ V and $I_o = 0.35$ A: (a) switch S_1 and diode D_1, (b) current i_{Lr1}, current i_{Lr2} and voltage C_r.

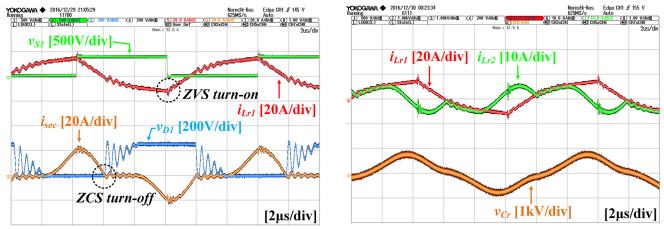

(a) (b)

Fig. 13. Experimental waveforms at $V_o = 250$ V and $I_o = 7$ A: (a) switch S_1 and diode D_1, (b) current i_{Lr1}, current i_{Lr2}, and voltage C_r.

not suitable for wide output voltage range application. The PRC and LCC resonant converters are able to control output voltage at light load. However, the rectifier diode is turned OFF with hard switching, and the operating frequency range is not sufficiently narrow under wide output voltage range. The LLC resonant converter is able to achieve not only ZVS turn-ON of primary switches, but ZCS turn-OFF of the rectifier diodes. However, the operating frequency range of the LLC resonant converter is too wide to be used under wide output voltage range. It should be noted that only the proposed converter has sufficiently narrow operating frequency range under wide output voltage range, thereby leading to reduced loss and cost of the magnetic components and auxiliary circuits such as gate driver and micro controller. The proposed converter achieves ZCS turn-OFF of the rectifier diodes as well as ZVS turn-ON of primary switches. Further, the proposed converter has no start-up problem unlike the other resonant converters since zero voltage gain is achieved at notch resonant frequency.

III. Experimental Result

A 3-kW laboratory prototype of the proposed converter has been built and tested to verify the proposed concept. The specification of the proposed converter is given in Table I. Component ratings and selected devices of the proposed converter are listed in Table V.

Figs. 12–14 show experimental waveforms under different output voltages of 50 V(point A, 160 kHz), 250 V(point B, 89 kHz), and 430 V(point D, 85 kHz), respectively. It is seen from the experimental results that switch S_1 is turned ON with ZVS, and diodes D_1 is turned OFF with ZCS regardless of voltage and load variation. The oscillations were caused by resonance between MOSFET's output capacitance and parasitic

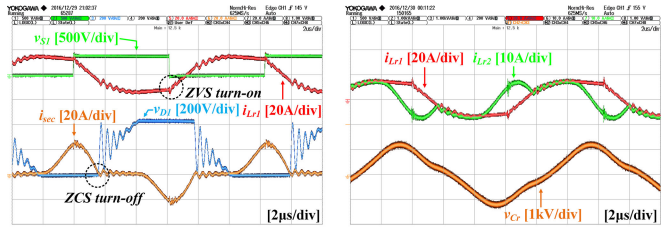

(a) (b)

Fig. 14. Experimental waveforms at $V_o = 430$ V and $I_o = 7$ A: (a) switch S_1 and diode D_1, (b) current i_{Lr1}, current i_{Lr2}, and voltage C_r.

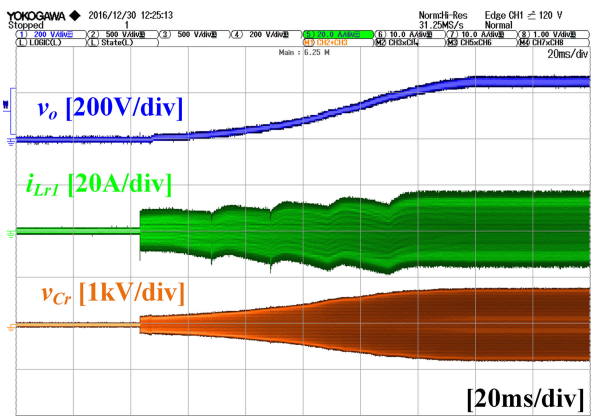

Fig. 15. Experimental waveforms of output voltage v_o, current i_{Lr1}, and voltage v_{Cr} during start-up.

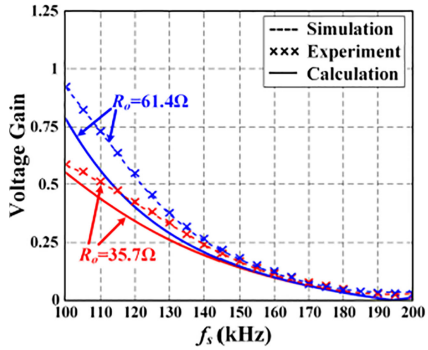

Fig. 16. Voltage gain curves obtained from the simulation, experiment, and calculation.

inductances in PCB pattern. This could be reduced by professional manufacturing techniques. Fig. 15 shows experimental waveforms of v_o, i_{Lr1} and v_{Cr} during start-up. Note that there are no voltage and current stresses in the resonant tank during start-up. This is because the proposed converter can start from zero voltage due to the notch resonant tank. Fig. 16 shows voltage gain curves obtained from the simulation, experiment, and calculation. The efficiencies for constant current and constant voltage modes are shown in Fig. 17(a) and (b), respectively. The maximum measured efficiency of the proposed converter is 96.8% at 3 kW when output voltage is 430 V. Fig. 18 shows calculated loss distribution of the proposed converter at full load

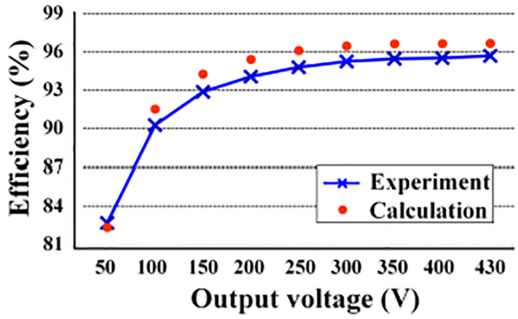

(a)

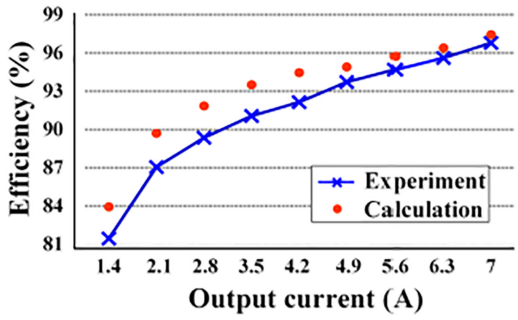

(b)

Fig. 17. Calculated and measured efficiencies (a) CC mode at $I_o = 7$ A. (b) CV mode at $V_o = 430$ V.

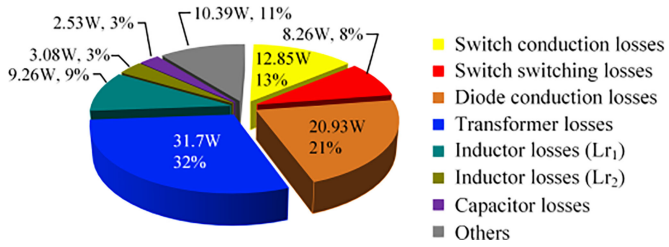

Fig. 18. Loss distribution of the proposed converter at full load ($V_o = 430$ V).

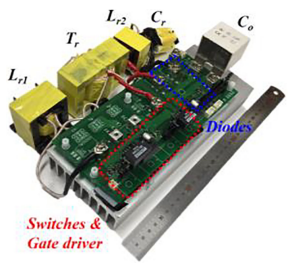

Fig. 19. Photograph of the proposed converter prototype.

when output voltage is 430 V. The efficiency is measured by YOKOGAWA WT3000.The large portion of the losses comes from the transformer and switching devices which are 32% and 42% of the total loss, respectively. Fig. 19 shows the photograph of the proposed prototype.

IV. Conclusion

In this paper, a new parallel loaded resonant converter is proposed for wide output voltage application such as eco-friendly vehicles and renewable energies. The proposed converter features narrow operating frequency range, ZVS turn-ON of switches and ZCS turn-OFF of diodes regardless of voltage and load variation. In addition, the resonant capacitor with feasible capacitance and current rating can be selected by utilizing the tertiary winding turn ratio of the transformer, thereby making the proposed converter more realizable in high power application. Furthermore, zero voltage gain can be achieved at notch resonant frequency, which can eliminate voltage and current stress in the resonant tank during start-up. Experimental results from a 3-kW prototype are provided to validate the proposed concept.

References

[1] J. Lee, Y. Jeong, and B. Han, "An isolated DC/DC converter using high-frequency unregulated LLC resonant converter for fuel cell applications," *IEEE Trans. Power Electron.*, vol. 58, no. 7, pp. 2926–2934, Jul. 2011.

[2] R. Beiranvand, B. Rashidian, M. R. Zolghadri, and S. M. H. Alavi, "A design procedure for optimizing the LLC resonant converter as a wide output range voltage source," *IEEE Trans. Power Electron.*, vol. 27, no. 8, pp. 3749–3763, Aug. 2012.

[3] C. Chang, E. Chang, and H. Cheng, "A high-efficiency solar array simulator implemented by an LLC resonant DC–DC converter," *IEEE Trans. Power Electron.*, vol. 28, no. 6, pp. 3039–3046, Jun. 2013.

[4] F. Musavi, M. Craciun, D. S. Gautam, W. Eberle, and W. G. Dunford, "An LLC resonant DC–DC converter for wide output voltage range battery charging applications," *IEEE Trans. Power Electron.*, vol. 28, no. 12, pp. 5437–5445, Dec. 2013.

[5] R. W. Erickson and D. Maksimovic, *Fundamentals of Power Electronics*, 2nd ed. Boulder, CO, USA: Kluwer, 2001.

[6] D. Huang, F. C. Lee, and D. Fu, "Classification and selection methodology for multi-element resonant converters," in *Proc. Conf. Expo. IEEE Appl. Power Electron.*, Mar. 2011, pp. 558–565.

[7] B. C. Hyeon and B. H. Cho, "Analysis and design of the LmC resonant converter for low output current ripple," *IEEE Trans. Power Electron.*, vol. 59, no. 7, pp. 2772–2780, Jul. 2012.

[8] G. Ivensky, S. Bronshtein, and A. Abramovitz, "Approximate analysis of resonant LLC DC-DC converter," *IEEE Trans. Power Electron.*, vol. 26, no. 11, pp. 3274–3284, Nov. 2011.

[9] J. Kim and G. Moon, "A new LLC series resonant converter with a narrow switching frequency variation and reduced conduction losses," *IEEE Trans. Power Electron.*, vol. 29, no. 8, pp. 4278–4287, Aug. 2014.

[10] J. Deng, S. Li, S. Hu, C. C. Mi, and R. Ma, "Design methodology of LLC resonant converters for electric vehicle battery chargers," *IEEE Trans. Veh Technol.*, vol. 63, no. 4, pp. 1581–1592, May 2014.

[11] J. Deng, C. C. Mi, R. Ma, and S. Li, "Design of LLC resonant converters based on operation-mode analysis for level two PHEV battery chargers," *IEEE/ASME Trans. Mechatron.*, vol. 20, no. 4, pp. 1595–1606, Aug. 2015.

[12] Z. Fang, T. Cai, S. Duan, and C. Chen, "Optimal design methodology for LLC resonant converter in battery charging applications based on time-weighted average efficiency," *IEEE Trans. Power Electron.*, vol. 30, no. 10, pp. 5469–5483, Oct. 2015.

[13] N. Shafiei and M. Ordonez, "Improving the regulation range of EV battery chargers with L3C2 resonant converters," *IEEE Trans. Power Electron.*, vol. 30, no. 6, pp. 3166–3184, Jun. 2015.

[14] R. Beiranvand, M. R. Zolghadri, B. Rashidian, and S. M. H. Alavi, "Optimizing the LLC–LC resonant converter topology for wide-output-voltage and wide-output-load applications," *IEEE Trans. Power Electron.*, vol. 26, no. 11, pp. 3192–3204, Nov. 2011.

[15] B. Lee, J. Kim, S. Kim, and J. Lee, "A PWM SRT DC/DC converter for 6.6-kW EV onboard charger," *IEEE Trans. Ind. Electron.*, vol. 63, no. 2, pp. 894–902, Feb. 2016.

[16] X. Xie, J. Zhang, C. Zhao, Z. Zhao, and Z. Qian, "Analysis and optimization of LLC resonant converter with a novel over-current protection circuit," *IEEE Trans. Power Electron.*, vol. 22, no. 2, pp. 435–443, Mar. 2007.

[17] W. Feng and F. C. Lee, "Optimal trajectory control of LLC resonant converters for soft start-up," *IEEE Trans. Power Electron.*, vol. 29, no. 3, pp. 1461–1468, Mar. 2014.
[18] R. Zheng, B. Liu, and S. Duan, "Analysis and parameter optimization of start-up process for LLC resonant converter," *IEEE Trans. Power Electron.*, vol. 30, no. 12, pp. 7113–7122, Dec. 2015.
[19] H. Wu, X. Jin, H. Hu, and Y. Xing, "Multielement resonant converters with a notch filter on secondary side," *IEEE Trans. Power Electron.*, vol. 31, no. 6, pp. 3999–4004, Jun. 2016.
[20] T. Mishima, H. Mizutani, and M. Nakaoka, "A sensitivity-improved PFM LLC resonant full-bridge DC–DC converter with LC antiresonant circuitry," *IEEE Trans. Power Electron.*, vol. 32, no. 1, pp. 310–324, Jan. 2017.
[21] F. Musavi, M. Craciun, D. S. Gautam, and W. Eberle, "Control strategies for wide output voltage range LLC resonant DC-DC converters in battery chargers," *IEEE Trans. Veh. Tech.*, vol. 63, no. 3, pp. 1117–1125, Mar. 2014.
[22] E. Asa, K. Colak, and D. Czarkowski, "Analysis of a CLL resonant converter with semi-bridgeless active rectifier and hybrid control," *IEEE Trans. Ind. Electron.*, vol. 62, no. 11, pp. 6877–6886, Nov. 2015
[23] I. O. Lee, "Hybrid DC/DC converter with phase-shift or frequency modulation for NEV battery charger," *IEEE Trans. Ind. Electron.*, vol. 63, no. 2, pp. 884–893, Feb. 2016.
[24] N. Shafiei, M. Ordonez, M. Craciun, C. Botting, and M. Edington, "Burst mode elimination in high-power LLC resonant battery charger for electric vehicles," *IEEE Trans. Power Electron.*, vol. 31, no. 2, pp. 1173–1188, Feb. 2016.
[25] H. Wu, Y. Li, and Y. Xing, "LLC resonant converter with semiactive variable-structure rectifier(SA-VSR) for wide output voltage range application," *IEEE Trans. Ind. Electron.*, vol. 31, no. 5, pp. 3389–3394, May 2016.
[26] G. Liu, Y. Jang, M. M. Jovanovic, and J. Q. Zhang, "Implementation of a 3.3-kW DC–DC converter for EV on-board charger employing the series-resonant converter with reduced-frequency-range control," *IEEE Trans. Ind. Electron.*, vol. 32, no. 6, pp. 4168–4184, Jun. 2017.
[27] H. Wu, X. Zhan, and Y. Xing, "Interleaved LLC resonant converter with hybrid rectifier and variable-frequency plus phase-shift control for wide output voltage range applications," *IEEE Trans. Ind. Electron.*, vol. 32, no. 6, pp. 4246–4257, Jun. 2017.
[28] H. Wu, T. Xia, X. Zhan, and Y. Xing, "High step-up isolated resonant converter with voltage quadrupler rectifier and dual-phase-shift control," *IEF Power Electron.*, vol. 8, no. 12, pp. 2462–2470, Dec. 2015.
[29] H. Wu, T. Xia, X. Zhan, P. Xu, and Y. Xing, "Resonant converter with resonant-voltage-multiplier rectifier and constant frequency phase-shift control for isolated buck-boost power conversion," *IEEE Trans. Ind. Electron.*, vol. 62, no. 11, pp. 6974–6985, Nov. 2015.
[30] C. C. Hua, Y. H. Fang, and C. W. Lin, "LLC resonant converter for electric vehicle battery chargers," *IEF Power Electron.*, vol. 9, no. 12, pp. 2369–2376, Oct. 2016.
[31] H. P. Park and J. H. Jung, "PWM and PFM hybrid control method for LLC resonant converters in high switching frequency operation." *IEEE Trans. Ind. Electron.*, vol. 64, no. 1, pp. 253–263, Jan. 2017.

Minjae Kim received the B.S.and M.S. and Ph. D. degrees from the New Energy Engineering, Seoul National University of Science and Technology (Seoul Tech), Seoul, Korea, in 2011 and 2013 and 2016, respectively.

In 2017, he joined the New Power Plasma Co., Ltd., Pyeongtaek, South Korea. His research interests include resonant converter for remote plasma source and battery charger for electric vehicles.

Hyeonju Jeong was born in Korea in 1989. He received the B.S. degree from the Department of Electronics and Electrical Engineering, Dankook University, Yongin, Korea, in 2014, and the M.S. degree from the Department of Electrical and Information Engineering, Seoul National University of Science and Technology (Seoul Tech), Seoul, Korea, in 2016. He is currently working toward the Ph.D. degree in Electrical and Information Engineering, Seoul Tech, Seoul, Korea.

His research interests include bidirectional dc–dc converter and resonant converter for electric vehicles and renewable energy systems.

Byeonggill Han received the B.S. degree in control and instrumentation Engineering from Hanbat National University, Daejeon, Korea, in 2016. He is currently working toward the M.S. degree at the Power Electronics & Fuel cell power Conditioning Laboratory, Seoul Tech.

His research interests include dc–dc converter and battery charger for electric vehicles.

Sewan Choi (S'92–M'96–SM'04) received the B.S. degree in electronic engineering from Inha University, Incheon, South Korea, in 1985, and the M.S. and Ph.D. degrees in electrical engineering from Texas A&M University, College Station, TX, USA, in 1992 and 1995, respectively.

From 1985 to 1990, he was with Daewoo Heavy Industries as a Research Engineer. From 1996 to 1997, he was a Principal Research Engineer at Samsung Electro-Mechanics Co., South Korea. In 1997, he joined the Department of Electrical and Information Engineering, Seoul National University of Science and Technology (Seoul Tech), Seoul, South Korea, where he is currently a Professor. His research interests include power conversion technologies for renewable energy systems and dc–dc converters and battery chargers for electric vehicles. He is an Associate Editor of the IEEE TRANSACTIONS ON POWER ELECTRONICS and IEEE JOURNAL ON EMERGING AND SELECTED TOPICS IN POWER ELECTRONICS.